JOURNAL OF SPACECRAFT AND ROCKETS
Vol. 33, No. 5, September–October 1996

Prediction of Hypersonic Shock-Wave/ Turbulent Boundary-Layer Interactions

Brian R. Smith*
Lockheed Martin Tactical Aircraft Systems, Fort Worth, Texas 76101

Predictions of two- and three-dimensional, Mach 8 shock-wave/turbulent boundary-layer interactions with a Navier–Stokes solver are presented. A $k-l$ two-equation turbulence model is used in the calculations. The two-dimensional cases are shock impingements generated by 5- and 10-deg wedges on a well-developed turbulent boundary layer. The three-dimensional case is a crossing shock flow generated by two symmetric 15-deg wedges. Results are compared to experimental surface pressure and heat transfer data and show good agreement. The importance of a compressibility correction to the turbulent length-scale equation is demonstrated. The Navier–Stokes solver uses an upwind discretization of the convective fluxes. The code uses a planar relaxation solver and includes implicit viscous and turbulence source terms. The turbulence model and Navier–Stokes equations are fully coupled in the flow solver.

Nomenclature

B_1, E_2, S_q	= turbulence-model transport equation constants
C_1, C_2	= turbulent viscosity constants
f_1	= term in turbulence-model damping function t
k	= turbulent kinetic energy
L	= wall proximity function, distance to nearest wall
l	= turbulent length scale
P	= turbulent production
$\boldsymbol{q}$	= flow-equation variable vector
q^2	= $2k$
$\boldsymbol{R}$	= transport-equation residual vector
S_{ij}	= mean-velocity strain tensor
U_i	= Favre-averaged mean-velocity component
u_i	= fluctuating velocity component
y^+	= near-wall viscous scaling, $y^+ = yu_\tau\rho/\mu$
δ_{ij}	= Kronecker delta
κ	= von Kármán constant
μ	= molecular viscosity
μ_t	= turbulent viscosity
ρ	= density
Φ	= turbulent viscosity damping function
χ	= turbulent viscosity function, $\chi = \rho ql/(B_1^{1/3}\mu)$
Ψ, α, r	= functions for turbulent viscosity limiter

Superscript

n	= iteration level

Introduction

IF computational fluid dynamics (CFD) is to be used in the design of hypersonic inlets, an understanding of the hypersonic shock-wave/turbulent boundary-layer interactions is critical to accurate prediction of heat loads, inlet efficiency, and drag. Through the study of shock-wave/turbulent boundary-layer interactions with well-documented experimental data, the accuracy of CFD calculations of flows closely related to inlet flowfields can be assessed and improved.

Turbulence modeling is a critical factor in the accurate prediction of hypersonic shock-wave/boundary-layer interactions. In this study, the $k-l$ two-equation turbulence model[1] is tested. This model consists of transport equations for the turbulent kinetic energy and the turbulent length scale. A near-wall model is included to accurately predict turbulence and velocity in the viscous sublayer and buffer regions. The turbulent-length-scale equation is much easier to resolve numerically than are the turbulent dissipation and turbulent vorticity equations used in the $k-\varepsilon$ and $k-\omega$ models, respectively.

Models that adequately predict transonic shock-wave/turbulent boundary-layer interactions are frequently far less accurate for hypersonic interactions. For transonic flows, predictions with the $k-l$ model are similar to predictions with other two-equation turbulence models, including the $k-\varepsilon$ model. For hypersonic flat-plate boundary-layer flows, $k-l$ model velocity profiles transformed using the van Driest compressibility relation agree well with the incompressible law of the wall, whereas $k-\varepsilon$ profiles do not. The van Driest transformation collapses experimental high-speed flat-plate velocity profiles well.[2,3] The primary motivation for this study is to test how accurately the $k-l$ model predicts more complex hypersonic flows.

The interactions chosen for this study, from the experimental investigations of Kussoy and Horstman,[4] are two-dimensional, wedge-generated, shock impingements on fully developed turbulent boundary layers, and a three-dimensional, symmetric crossing-shock-wave interaction generated by 15-deg wedges.[5,6] One of the two-dimensional interactions contains a small region of separation. Surface pressure and heat transfer data are available for comparison. The three-dimensional interaction contains small regions of separation and large regions of shock-induced vortical flow. Calculations and measurements of surface pressure, heat transfer, and pitot pressure are made. In addition, the simulated and experimental oil flows are compared.

Horstman[7] compared the prediction of several two-equation models with compressibility corrections to the two-dimensional interactions of Kussoy and Horstman,[4] and Narayanswami et al.[8] compared an algebraic model and a two-equation model to the three-dimensional crossing-shock interaction.[5] Bardina and Coakley[9] also tested several versions of the $k-\varepsilon$ and $k-\omega$ two-equation models on the 15-deg crossing-shock problem. These published computational investigations provide a benchmark for evaluation of the predictions from the current investigation with the $k-l$ model.

The $k-l$ model is implemented in an implicit, planar-relaxation Navier–Stokes solver. A secondary motivation of this study is to determine the efficiency and robustness of the $k-l$ model with the planar-relaxation solver for complex hypersonic turbulent flows.

Experimental Flows

All of the interactions in this study were tested in the NASA Ames Research Center 3.5-ft hypersonic wind tunnel under similar conditions, summarized in Table 1. A turbulent boundary layer with natural transition well upstream of the interactions develops over a 1.5-m-long flat plate with a sharp leading edge. Figure 1 shows the

Received Jan. 23, 1995; revision received May 13, 1996; accepted for publication May 26, 1996.

*Engineering Group Specialist, Computational Fluid Dynamics Group, P.O. Box 748, MZ 9333. Member AIAA.

Table 1 Summary of experimental flow conditions

	Two-dimensional wedge generator	Three-dimensional crossing shock
Mach	8.18	8.28
T_∞, °R	146	144
T_t, °R	2097	2118
T_w/T_t	0.257	0.255
P_∞, psf	9.0	9.0
Re/ft	1.5×10^6	1.6×10^6

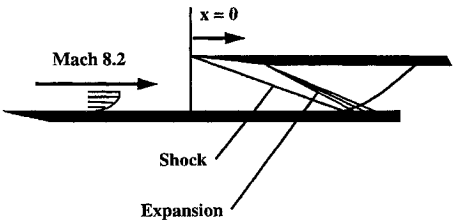

Fig. 1 Two-dimensional shock-wave/boundary-layer interaction.

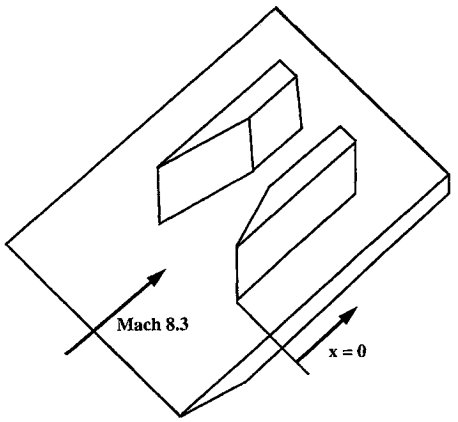

Fig. 2 Three-dimensional crossing-shock-wave interaction.

basic two-dimensional interaction. The 5- and 10-deg wedge-shock generator cases were chosen for analysis. Separation is present with the 10-deg wedge, but not for the 5-deg case.[4] The three-dimensional crossing-shock flow is shown in Fig. 2 (Refs. 5 and 6).

A relatively small portion of the test bed was instrumented for both tests. To obtain results over the entire interaction region, the wedges were displaced in the x direction. As a result, the full experimental data set for each case was obtained in multiple runs with different upstream boundary-layer thicknesses.

Computational Method

The planar-relaxation FALCON (PRFALCON) Navier–Stokes code is used for the calculations. The code uses a marching algorithm in the i direction and approximate factorization in the j and k directions. The code can be run in parabolized Navier–Stokes (PNS) mode to initialize the flowfield. This solution approach is extremely well suited to hypersonic flow when the i direction in computational space is approximately aligned with the dominant flow direction, because the downstream influence is only present in the boundary layer very close to the wall. Flow variables and residuals are updated and used as the solution is marched in the $+i$ direction, $\boldsymbol{R}_i^n = f(\boldsymbol{q}_{i-1}^{n+1}, \boldsymbol{q}_i^n, \boldsymbol{q}_{i+1}^n)$. Other iteration schemes are available in the flow solver. The code is highly vectorized and has multiple block capability.

PRFALCON uses second-order, upwind differencing of the convective fluxes with finite volume discretization. Roe's flux-difference-split scheme[10] is used, with the minmod limiter. The entropy fix of Van Leer is applied to prevent development of expansion shocks.[11] For this study the perfect-gas assumption is used.

The Navier–Stokes and $k-l$ turbulence model left-hand-side flux Jacobians are coupled, resulting in a 7×7 block tridiagonal system for the AF scheme. Approximate, first-order, left-hand-side convective flux Jacobians are derived from Roe's scheme; the Roe Jacobian matrix is not differentiated. Viscous, turbulent-source, and implicit boundary Jacobians are included in the implicit treatment. To increase code stability, the diagonal terms of the $k-l$ model source Jacobians are set to zero if they decrease diagonal dominance. A variable time step is used for the steady-state calculations to accelerate convergence. By coupling the Navier–Stokes and turbulence-model equations in an implicit solution algorithm, large time steps and high rates of convergence are made possible.

Turbulence Modeling

The $k-l$ model was derived from a $k-kl$ model.[12] Transformation of the kl transport equation to an l equation eliminates several near-wall terms and results in an equation that is easier to handle numerically. Two modifications to the Smith[1] $k-l$ model have been made to improve predictions of highly compressible flows. These changes are included in Eqs. (1) and (2). The model transport equations for ρq^2, where $q^2 = 2k$, and ρl are

$$\frac{\partial \rho q^2}{\partial t} + \frac{\partial \rho q^2 U_i}{\partial x_i} = 2P - \frac{2\rho q^3}{B_1 l} - 2\mu \frac{\partial q}{\partial x_i}\frac{\partial q}{\partial x_i} + \frac{\partial}{\partial x_i}(\mu + S_q \mu_t)\frac{\partial q^2}{\partial x_i} \tag{1}$$

$$\frac{\partial \rho l}{\partial t} + \frac{\partial \rho l U_i}{\partial x_i} = (2 - E_2)\frac{\rho q}{B_1}\left[1 - \left(\frac{l}{\kappa L}\right)^2\right] - \frac{\mu_t}{l} S_q \left(\frac{\partial l}{\partial x_i}\right)^2 \left(\frac{l}{\kappa L}\right)^2 + \rho l \frac{\partial u_i}{\partial x_i} + 2S_q\left(\frac{\mu_t}{q^2}\right)\frac{\partial l}{\partial x_i}\frac{\partial q^2}{\partial x_i} + \frac{\partial}{\partial x_i}(\mu + S_q \mu_t)\frac{\partial l}{\partial x_i} \tag{2}$$

The model has empirical constants $(B_1, E_2, S_q, \kappa) = (18.0, 1.2, 0.7, 0.41)$. The turbulence production is given by $P = \overline{\rho u_i u_j}\,(\partial U_i/\partial x_j)$. The Bousinesq approximation is used for the turbulent stresses, as shown in Eq. (3):

$$\overline{\rho u_i u_j} = \mu_t\left[\left(\frac{\partial U_i}{\partial x_j} + \frac{\partial U_j}{\partial x_i}\right) - \frac{2}{3}\left(\frac{\partial U_k}{\partial x_k}\right)\delta_{ij}\right] - \frac{\delta_{ij}}{3}\rho q^2 \tag{3}$$

For the calculations in this study, the turbulent viscosity definition of the $k-l$ model[1] was modified to prevent turbulent stresses defined by Eq. (3) from becoming unrealistically large in shock waves. The unmodified turbulent viscosity is defined in Eq. (4):

$$\mu_t' = \mu \chi \Phi \tag{4}$$

where

$$\chi = \frac{\rho q l}{\mu B_1^{\frac{1}{3}}} \qquad \Phi = \left(\frac{C_1^4 f_1 + C_2^2 \chi^2 + \chi^4}{C_1^4 + C_2^2 \chi^2 + \chi^4}\right)^{\frac{1}{4}}$$

$$f_1 = \exp[-50(l/\kappa L)^2]$$

The turbulent viscosity constants (C_1, C_2) are (25.5, 2.0) (Ref. 1).

In shock waves and strong compressions, Eq. (3) can give normal stresses that are larger than ρq^2, which is physically impossible. The limiting of the turbulent viscosity makes use of the relation

$$\rho^2 q^4 \geq \overline{\rho u_i u_j}\;\overline{\rho u_i u_j} \tag{5}$$

The turbulent viscosity modification function Ψ, shown in Eq. (6), guarantees that Eq. (5) is satisfied:

$$\mu_t = \Psi \mu_t' \tag{6}$$

where

$$\Psi = \frac{1}{(\alpha + r)^{\frac{1}{2}}} \qquad \alpha^2 = 1 - \frac{3}{2B_1^{\frac{4}{3}}}$$

$$r = \frac{3}{2}\frac{(\mu_t')^2 S_{ij} S_{ij}}{\rho^2 q^4} \qquad S_{ij} = \left(\frac{\partial U_i}{\partial x_j} + \frac{\partial U_j}{\partial x_i}\right) - \frac{2}{3}\left(\frac{\partial U_k}{\partial x_k}\right)\delta_{ij}$$

The quantity r is obtained by substituting the turbulent stress relation, Eq. (3), into Eq. (5). The constant α ensures that $\Psi = 1$ in the

logarithmic region of a turbulent boundary layer. Outside of shocks and strong compressions, Ψ has little effect.

The second compressibility modification to the $k - l$ turbulence model is the addition of the compressibility correction term to the length-scale equation. The term arises from the assumption that a compression of the mean flowfield reduces the size of turbulent eddies and, therefore, the length scale. Conversely, an expansion increases the size of the turbulent eddies and the length scale. This term has been applied successfully in other two-equation turbulence models.[13] Calculations were performed with and without this term to assess its usefulness. Favre mass-weighted averaging is employed. No other compressibility corrections are included in the $k - l$ model. Unlike the $k - \varepsilon$ model[7] and $k - \omega$ model,[13] no ad-hoc limiting of the turbulent length scale is required near separation points.

Computational Results

Table 2 summarizes the grid and near-wall spacing for all of the solutions. The boundary layer used in the upstream boundary

Table 2 Summary of computational grids

Case	Grid dimensions (streamwise × normal)	y^+ Bottom wall, upstream of interaction	y^+ Bottom wall, peak	y^+ Center of wedge
5-deg wedge, two dimensional	221 × 111	0.07	0.2	2.0
10-deg wedge, coarse, two dimensional	97 × 111	0.10	0.6	1.4
10-deg wedge, fine, two dimensional	167 × 161	0.09	0.6	1.0
Crossing shock, three dimensional	111 × 71 × 61	0.03	0.4	0.4

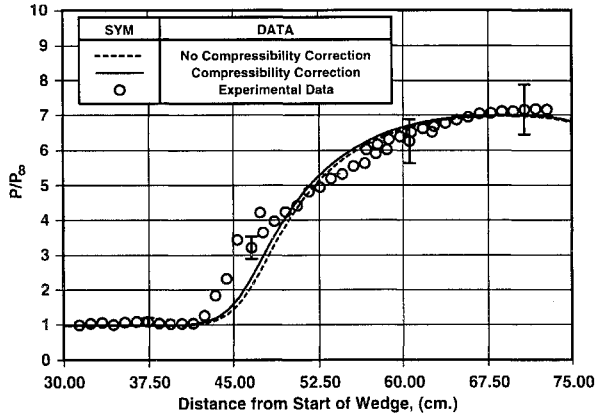

Fig. 3a Surface pressure for 5-deg wedge-shock-wave/boundary-layer interaction.

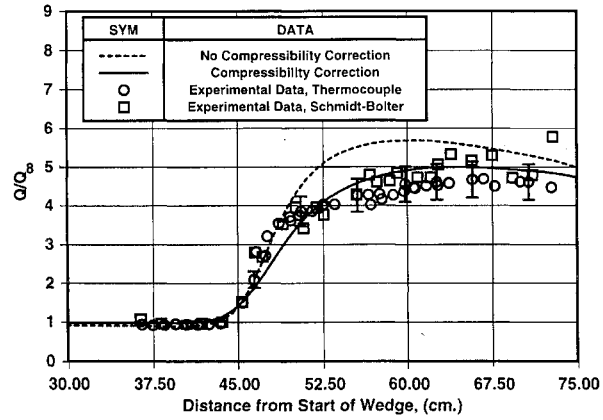

Fig. 3b Surface heat transfer for 5-deg wedge-shock-wave/boundary-layer interaction.

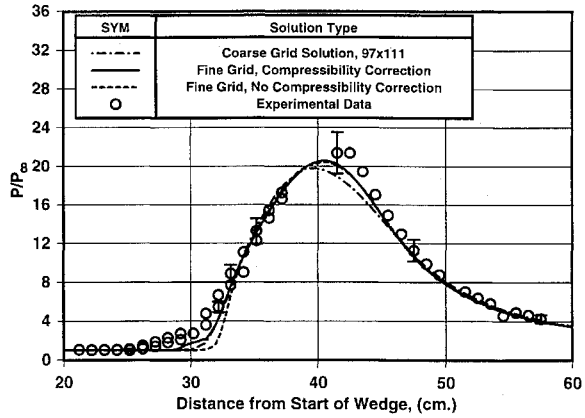

Fig. 4a Surface pressure for 10-deg wedge-shock-wave/boundary-layer interaction.

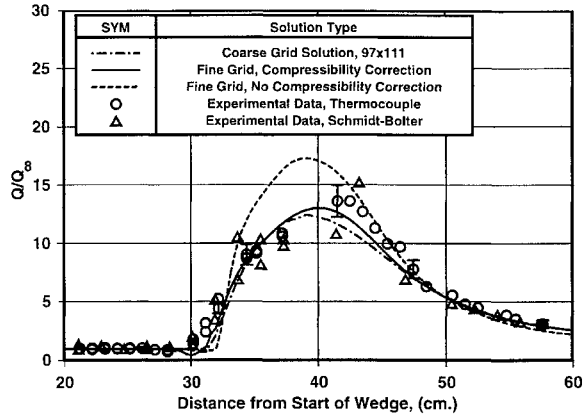

Fig. 4b Heat transfer for 10-deg wedge-shock-wave/boundary-layer interaction.

condition of the shock-wave/turbulent boundary-layer interaction solutions was obtained computationally. In calculating the incoming boundary layer, transition locations were adjusted to obtain the best possible fit to experimental velocity profiles on an undisturbed flat plate 187 cm from the leading edge. Transition onset was set at 50 cm and completion at 75 cm from the leading edge, in agreement with the 50- to 100-cm transition range found experimentally. The interaction region was between 105 and 200 cm from the leading edge for all experiments.

Two-Dimensional Interactions

The flow is attached for the 5-deg wedge-generated shock interaction. Figures 3a and 3b show the surface pressure and heat transfer, respectively, near the interaction. The computed results slightly underestimate the upstream extent of the interaction. Although the length-scale compressibility correction has little effect on the surface pressure, it improves agreement with the experimental heat transfer data. Without the compressibility correction, the turbulent length scale in the interaction region is too large, resulting in elevated heat transfer and skin friction. With the compressibility correction, computed heat transfer and surface pressure are within the error band of the experimental data, estimated to be ±10% by Kussoy and Horstman,[4] for most of the interaction. The thermocouples are believed to be more accurate than the Schmidt–Bolter gauges.

For the 10-deg wedge-generated shock interaction, a small separation region develops where the surface-pressure rise begins on the plate. Two different grid sizes were run for this case, 97 × 111 and 167 × 161. The solution domain begins at the shock generator and extends 61 cm downstream. Surface pressure and heat transfer for this case are shown in Figs. 4a and 4b, respectively. As in the 5-deg wedge case, the solution without the length-scale compressibility correction overpredicts the heat transfer in the interaction region.

The separated flow region is larger in the fine-grid solution than it is in the coarse-grid solution. The effect of the separation on the surface pressure can be seen in Fig. 4a. Because the distance between the leading edge and the expansion of the 10-deg wedge is half that of the 5-deg wedge, the peak pressure for the 10-deg wedge flow is more sensitive to numerical diffusion between the shock and the expansion. The fine-grid solution has a higher peak pressure and heat transfer. The fine-grid solution is nearly grid independent because additional solutions with grids adapted to the shocks did not affect the results. For this case, predictions with the $k - l$ model are better than the predictions of Horstman[7] using several different versions of the $k - \varepsilon$ model.

Three-Dimensional Crossing-Shock Interaction

The Mach 8 crossing-shock interaction flow is far more complex than the two-dimensional interaction flows. Lateral pressure gradients on the bottom wall caused by the wedge shocks result in large lateral variations of the boundary-layer thickness. These variations in the boundary-layer displacement change the shock structure and influence the pressure field.

The flowfield was computed by putting a symmetry plane along the centerline of the wedge flowfield. In the direction normal to the plate, the grid extended well outside the interaction region. The PRFALCON code was run in PNS mode to initialize the solution for Navier–Stokes mode. Starting from this well-initialized solution, approximately 300 iterations are required to reduce the residual norm of both the flow equations and the turbulence equations three additional orders of magnitude. No significant change in flowfield quantities occurs beyond this level of convergence. For this 480,000-grid-point problem, approximately 450 CPU seconds are required per iteration using a Cray Y-MP-EL. Approximately 30 CPU seconds are required per iteration using a Cray C90.

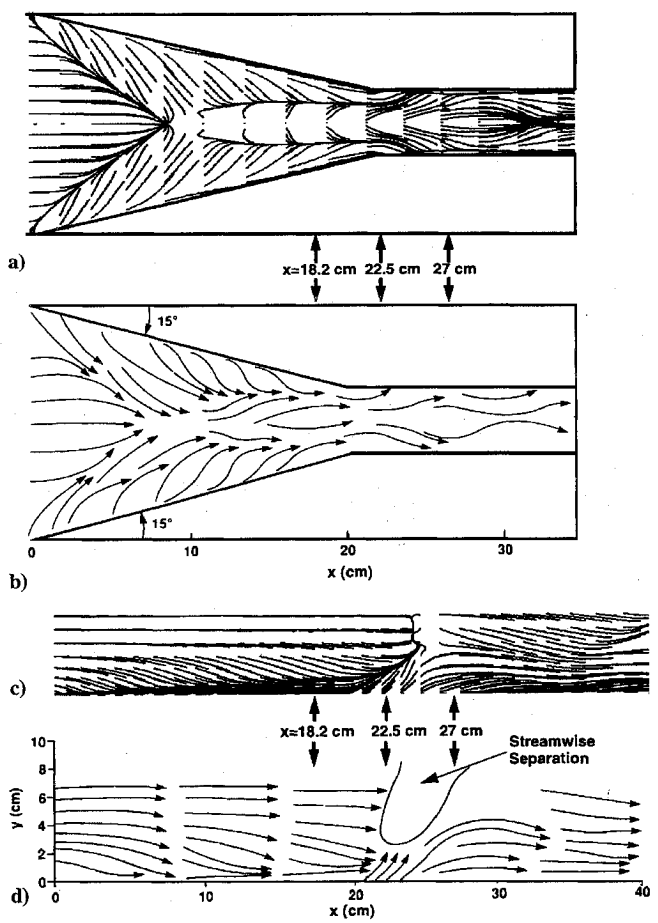

Fig. 5 Oil flow, 15-deg crossing-shock flow: a) simulated computationally, bottom plate; b) traced from experiment, bottom plate[6]; c) simulated computationally, wedge wall; and d) traced from experiment, wedge wall.[6]

Oil flows from the experiment and computation with the length-scale compressibility correction are shown in Fig. 5. The experimental results in Figs. 5b and 5d were traced from oil-flow photographs by Kussoy and Horstman,[6] and are reproduced here. Oil flows on the bottom plate are compared in Figs. 5a and 5b. The computational oil flow reflected about the symmetry plane agrees well with the experimental oil flow. The small region of streamwise separation on the centerline about 10 cm from the leading edge is evident in the calculated oil flow. The experimental and computational oil flows on the wedge wall (Figs. 5c and 5d) show good agreement. The calculated streamwise separation downstream of the corner is smaller than the experimental separation. The oil-flow comparisons show that the qualitative features of the flow are captured by the calculations. Although they are not shown here, the experimental and computational pitot pressures at three-cross-flow plane agreed well.

Experimental surface pressure and heat transfer data were taken along the centerline and laterally at three stations near the crossing-shock location. Figure 6 shows the surface pressures along the centerline (Fig. 6a) and at the three stations (Figs. 6b–6d). Agreement with experimental pressure measurements is very good. The reported accuracy of the experimental data is ±10% (Ref. 5). The peak surface pressure is within the accuracy of the experimental data. Overall, inclusion of the length-scale compressibility correction results in poorer agreement with the experimental surface pressures.

A comparison of the experimental and calculated heat transfer data is shown in Figs. 7a–7d. Agreement with the experimental data is only fair, particularly on the centerline (Fig. 7a). The peak heat transfer with the compressibility correction is almost 30% higher than the experimental level. Without the correction, the predicted centerline heat transfer is low. For the two-dimensional interactions, lower levels of heat transfer were predicted with the length-scale compressibility correction than without it. Away from the centerline (Figs. 7b–7d), the agreement with the experimental data is better for both solutions, and the solution with the compressibility correction gives better overall predictions of the heat transfer.

There are several possible experimental sources for the discrepancy between the computed and experimental heat transfer. Because Kussoy and Horstman[5] do not give an estimate of the effect of streamwise displacement of the wedges on their measurements, the effect was tested computationally. Streamwise displacement of the wedges causes changes in the boundary-layer thickness upstream of the interaction of up to 10%, resulting in changes of up to 10% in the pressure and heat transfer on the centerline. A second possible source of the discrepancy is the asymmetry in the experimental flow. Both the oil-flow traces on the bottom plate and the surface heat transfer measurements are asymmetric, although the asymmetry in the off-centerline heat transfer measurements is within the stated 10% experimental error range. This asymmetry could be caused by unsteadiness or by an asymmetry in the experimental setup. Because the calculated heat transfer has a relatively sharp peak near the centerline, any asymmetry in the flow could reduce the measured heat transfer on the centerline.

On the computational side, errors could be due to either grid resolution or turbulence modeling. This study uses a finer grid than was used in other published calculations of this flow.[8,9] Preliminary calculations using grids with poorer resolution did not differ greatly from the final calculations. Poor grid resolution is not likely the primary source of differences between calculation and experiment. Figures 6 and 7 clearly illustrate that the surface pressure and heat transfer are highly sensitive to the turbulence model. Further investigation of compressibility effects in turbulence models is warranted.

Significant differences are apparent when the current solutions are compared with the solutions of Narayanswami et al.[8] and Bardina and Coakley.[9] The calculations of Narayanswami et al. have local minima in the heat transfer along the centerline at stations 1 and 2, whereas the solutions of Bardina and Coakley and from this study have local maxima at the centerline. The solutions of Bardina and Coakley do not appear to be well resolved along the centerline. Only 41 grid points were used between the symmetry plane and the wedge in this calculation, resulting in underestimation of the magnitude of the local maxima along the centerline. As a result, the Bardina and Coakley results may underestimate the centerline heat transfer. For

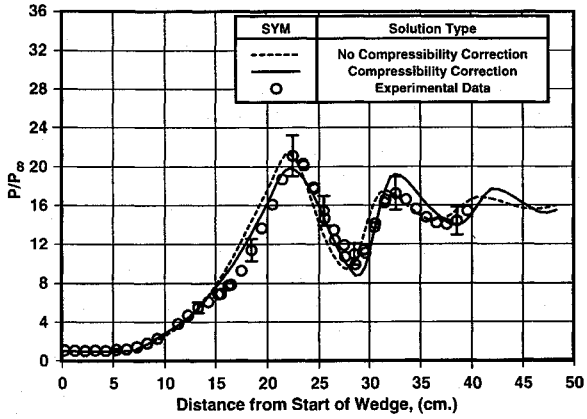

Fig. 6a Centerline surface pressure for 15-deg wedge-crossing-shock problem.

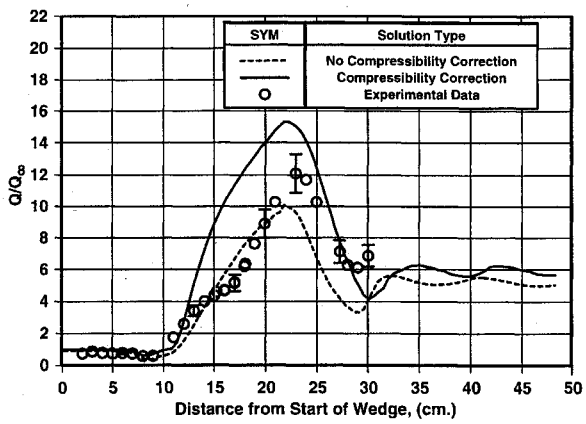

Fig. 7a Centerline heat transfer for 15-deg wedge-crossing-shock problem.

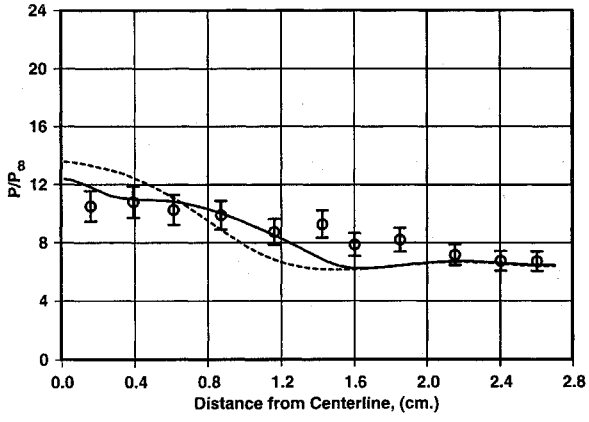

Fig. 6b Surface pressure at station 1, 18.2 cm.

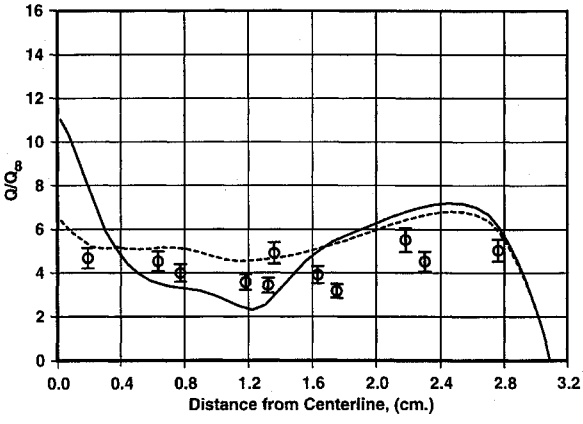

Fig. 7b Heat transfer at station 1, 16.5 cm.

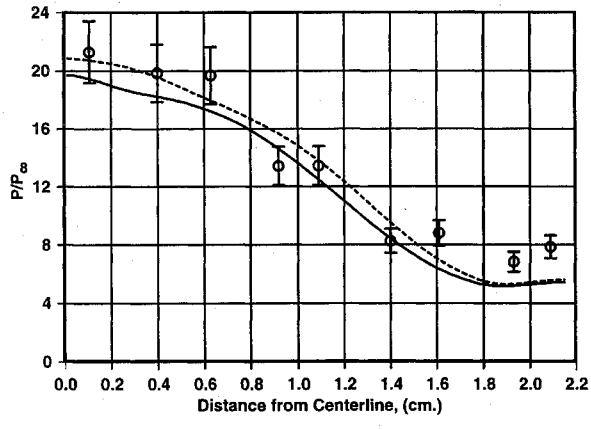

Fig. 6c Surface pressure at station 2, 22.5 cm.

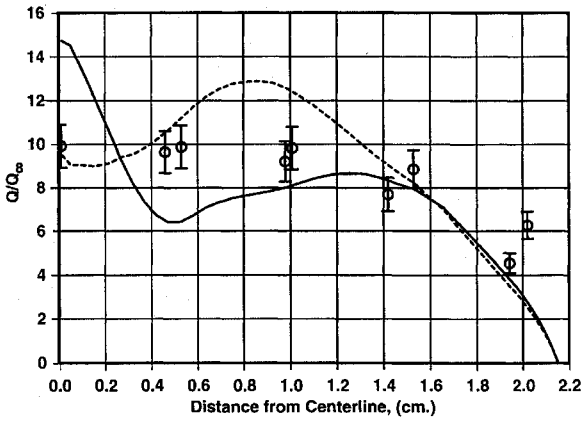

Fig. 7c Heat transfer at station 2, 20.8 cm.

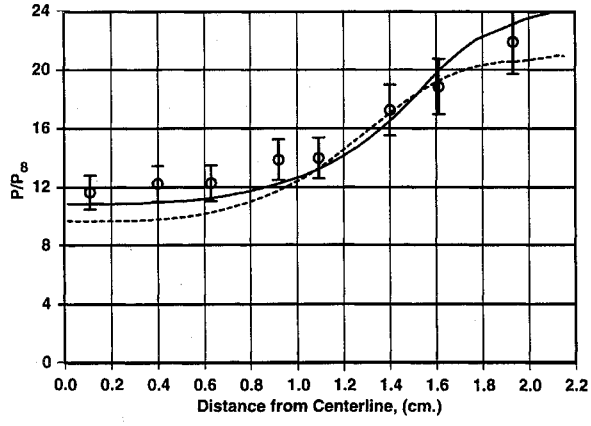

Fig. 6d Surface pressure at station 3, 27.0 cm.

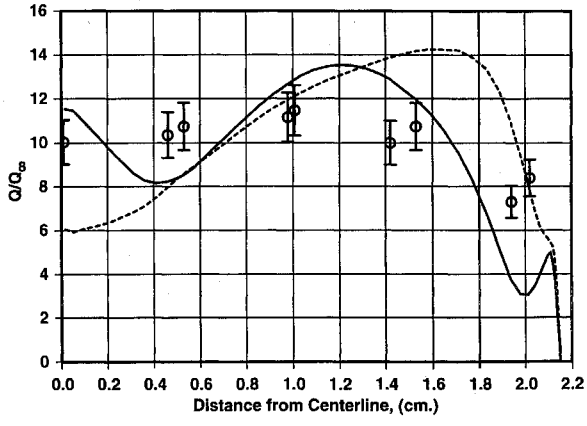

Fig. 7d Heat transfer at station 3, 25.3 cm.

the current study, 61 grid points were used in the direction normal to the wedge, and the grid was well clustered along the centerline.

In comparing the results using the $k-\varepsilon$, $k-\omega$ and Baldwin–Lomax models[8,9] to the results of the current study with the $k-l$ model, it is difficult to evaluate the effect of turbulence models because of differences in computational methods and grid resolution. The current calculations with the $k-l$ model appear to be as good as or better than the best predictions obtained in these other studies.

Assessment of Compressibility Correction

The length-scale compressibility correction term significantly improves predictions of heat transfer in two-dimensional shock-wave/boundary-layer interactions. It has very little effect on the surface pressure. In contrast, in the three-dimensional crossing-shock flow, the benefit of the length-scale correction is less clear. Along the centerline of the crossing-shock flow, a lower heat transfer was obtained without the compressibility correction. This result is opposite to the effect observed in the two-dimensional interactions. The centerline surface pressure is also more sensitive to the compressibility correction in the crossing-shock flow than it is in two-dimensional interactions.

These results emphasize the complexity of the relationship between the divergence of the velocity field and the turbulent length scale. In particular, flow compression normal to a wall, which occurs in the two-dimensional interactions, tends to reduce the turbulent length scale in the direction that dominates mixing and dissipation. In contrast, in the three-dimensional crossing-shock interaction, there is significant expansion in the lateral direction near the wall at the symmetry plane. This expansion is indicated by the divergence of the oil-flow lines near the symmetry plane shown in Fig. 5. Because the compressibility correction term does not differentiate between compressibility that is normal to a wall and compressibility that is lateral or streamwise, the term causes the turbulent length scale to grow near the wall at the centerline. An increase in the turbulent length scale increases turbulent mixing and turbulent heat transfer. In reality, expansion of turbulent eddies in the lateral direction would not tend to increase mixing and dissipation significantly. A more sophisticated length-scale compressibility term may be required for accurate predictions of three-dimensional shock-wave/turbulent boundary-layer interactions.

Conclusions

Good agreement has been obtained using the PRFALCON Navier–Stokes solver with the $k-l$ two-equation turbulence model for Mach 8 shock-wave/turbulent boundary-layer interactions. The principal conclusions of this study are as follows:

1) The $k-l$ turbulence model is accurate for hypersonic shock-wave/turbulent boundary-layer interactions.

2) The length-scale compressibility correction is more effective in two-dimensional interactions than it is in three-dimensional interactions.

3) The inclusion of implicit viscous and turbulent source terms and boundary conditions in the Navier–Stokes solver, and implicit coupling of the Navier–Stokes and turbulence equations results in a highly efficient solution algorithm for high-speed viscous flows.

Because the $k-l$ model is easy to resolve numerically and gives good results for hypersonic shock-wave/boundary-layer interactions, it is a good choice for use in hypersonic flow simulations.

References

[1]Smith, B. R., "A Near Wall Model for the $k-l$ Two Equation Turbulence Model," AIAA Paper 94-2386, June 1994.

[2]Huang, P. G., and Coleman, G. N., "Van Driest Transformation and Compressible Wall-Bounded Flows," *AIAA Journal*, Vol. 32, No. 10, 1994, pp. 2110–2113.

[3]Huang, P. G., Bradshaw, P., and Coakley, T. J., "Turbulence Models for Compressible Boundary Layers," *AIAA Journal*, Vol 32, No. 4, 1994, pp. 735–740.

[4]Kussoy, M. I., and Horstman, K. C., "Documentation of Two- and Three-Dimensional Shock-Wave/Turbulent-Boundary-Layer Interaction Flows at Mach 8.2," NASA TM 103838, May 1991.

[5]Kussoy, M. I., and Horstman, K. C., "Intersecting Shock-Wave/Turbulent Boundary-Layer Interactions at Mach 8.3," NASA TM 103909, Feb. 1992.

[6]Kussoy, M. I., and Horstman, K. C., and Horstman, C. C., "Hypersonic Crossing Shock-Wave/Turbulent-Boundary-Layer Interactions," *AIAA Journal*, Vol. 31, No. 12, 1993, pp. 2197–2203.

[7]Horstman, C. C., "Hypersonic Shock-Wave Turbulent Boundary Layer Interaction Flows—Experiment and Computation," AIAA Paper 91-1760, June 1991.

[8]Narayanswami, N., Horstman, C. C., and Knight, D. D., "Computation of Crossing Shock/Turbulent Boundary Layer Interaction at Mach 8.3," *AIAA Journal*, Vol. 31, No. 8, 1993, pp. 1369–1376.

[9]Bardina, J. E., and Coakley, T. J., "Three-Dimensional Navier–Stokes Simulations with Two-Equation Turbulence Models of Intersecting Shock-Wave/Turbulent Boundary Layer at Mach 8.3," AIAA Paper 94-1905, June 1994.

[10]Roe, P. L., "Characteristic-Based Schemes for the Euler Equations," *Annual Review of Fluid Mechanics*, Vol. 18, 1986, pp. 337–365.

[11]Van Leer, B., Lee, W., and Powell, K. G., "Sonic-Point Capturing," *AIAA 9th Computational Fluid Dynamics Conference*, AIAA, Washington, DC, 1989, pp. 176–187 (AIAA Paper 89-1945).

[12]Smith, B. R., "The $k-kl$ Turbulence Model and Wall Layer Model for Compressible Flows," AIAA Paper 90-1483, June 1990.

[13]Coakley, T. J., Horstman, C. C., Marvin, J. G., Viegas, J. R., Bardina, J. E., Huang, P. G., and Kussoy, M. I., "Turbulence Compressibility Corrections," NASA TM 108827, May 1994.

J. C. Adams
Associate Editor